Experimental observations of nonlinear vibration localization in a cyclic chain of weakly coupled nonlinear oscillators

B. Niedergesäß[a,*], A. Papangelo[a,b], A. Grolet[c], A. Vizzaccaro[d], F. Fontanela[d], L. Salles[d], A.J. Sievers[e], N. Hoffmann[a,d]

[a] Hamburg University of Technology, Department of Mechanical Engineering, Am Schwarzenberg-Campus 1, Hamburg 21073, Germany
[b] Politecnico di Bari. Department of Mechanics, Mathematics and Management, Via Orabona 4, Bari 70125, Italy
[c] École Nationale Superieure d'Arts et Métiers, Department of Mechanical Engineering, Lille, France
[d] Imperial College London, Department of Mechanical Engineering, Exhibition Road, London SW7 2AZ, UK
[e] Cornell University, Laboratory of Atomic & Solid Physics, 317 Clark Hall, Ithaca, NY 14853-2501, USA

ARTICLE INFO

Article history:
Received 10 July 2020
Revised 26 November 2020
Accepted 14 January 2021
Available online 15 January 2021

Keywords:
Vibration localization
Clearance
Cyclic structure

ABSTRACT

Experimental results on nonlinear vibration localization in a cyclic chain of weakly coupled oscillators with clearance nonlinearity are reported. Numerical modelling and analysis complements the experimental study. A reduced order model is derived and numerical analysis based on the harmonic balance method demonstrates the existence of multiple classes of stable spatially localized nonlinear vibration states. The experiments agree very well with the numerical results. The findings suggest that vibration localization due to fundamentally nonlinear effects may also arise in mechanical structures with relevance in engineering.

1. Introduction

Reducing the vibration amplitude of engineering structures is a common goal for designers, who aim at improving fatigue life, reducing wear and maintenance costs. In particular, in aerospace and aeronautical engineering vibration mitigation of complex structures such as turbines [1–6], reflectors and antennas [7,8] is a critical and often highly non-trivial task [9]. The mechanical structures concerned are composed of ideally identical elements assembled in a cyclic fashion. In such systems cyclic symmetry is sought for dynamic balancing of rotating structures and to equally distribute energy preventing fatigue and degradation of individual components. Assuming linearity, structural symmetry usually amounts to a symmetric, spatially homogeneous response under spatially homogeneous excitation. Underlying are modal deformation patterns in the form of standing waves, varying periodically in the circumferential direction. Deviations from a spatially homogeneous response, which often manifest themselves in the form of locally amplified vibration amplitudes, are usually attributed to symmetry-breaking inhomogeneities of the structure. The discovery of linear localized vibration modes dates back to the early works in solid state physics by Lifshitz [18], who studied the vibrational properties of inhomogeneous crystal lattice, and by Anderson [19] who showed that inhomogeneities may strongly influence lattice transport properties. In turbomachinery the effect of vibration localization due to inhomogeneities or symmetry breaking may often be found under the name ‘mistuning’, relating the inhomogeneity to spectrally inhomogeneous sectors of the rotors, usually blades [10–15].

In engineering, considerable effort has been made theoretically and numerically to estimate the maximum vibration amplification in bladed disks due to mistuning [12–15], nevertheless erosion and wear during service may result in geometrical variations which are often difficult to account for. However, structures often also exhibit nonlinear effects, which may lead to various localization mechanisms [20–28]. Turbines in aero-engines, for example, may comprise nonlinearities due to internal mechanical joints, high amplitude response, or geometrical effects like clearances [2–5,14–17,29]. Especially the need for new lightweight designs may increase these effects even further as slender structures may undergo large deformation during operation [28] and might require more sophisticated damping strategies. In the nonlinear regime vibration localization driven by nonlinear effects, and not inhomomogeneity, may arise due to the dependency of modal properties on response amplitude. Through internal resonances nonlinear modes may interact and confine energy to a distinct part of the system [20–24,30]. In physics, analogous localized states are referred to as Intrinsic Localized Modes (ILM) or Discrete Breathers (DB) [31–34]. It has already been shown theoretically and numerically that in both self-excited [25,26] and externally-excited [27,28] nonlinear homogeneous weakly coupled structures the vibration energy may strongly localize in space (see also [22,37–41]). For a given set of system parameters, multiple coexisting stable and unstable states have been detected [26,35,36], which may also respond in the form of regular or irregular vibrations [42,43] (so called “chimera states”) and in terms of bifurcation diagrams give rise to snaking-like patterns, similarly to what has been observed in other fields of physics such as fluid dynamics [44,46,47] and nonlinear optics [44].

The aim of this paper is to move the question on nonlinear vibration localization a step closer to realistic engineering-like structures. Following earlier work on localization in a non-cyclic system of two coupled oscillators [45], here a cyclic chain of three weakly coupled oscillators with on-site clearance nonlinearity is considered. First, in Section 2 the reader is introduced to a lumped model with the aim to show how the phenomenon of vibration localization takes place due to the bistability of the single oscillator that composes the cyclic symmetric chain. The lumped model retains the essential features of the experimental structure but without the uncertainties related to the real component (e.g. manufacturing tolerances and damping). Numerical simulations are conducted by means of the harmonic balance method together with numerical continuation, which show a multiplicity of localized coexisting stable and unstable states. Then an experimental cyclically symmetric test rig is presented, which consists of three weakly coupled slender beams with clearance nonlinearity. By measuring the system response at different excitation frequencies and excitation amplitudes, spatially localized vibration is detected and characterized. It is shown that the localized states are stable in time and robust, so that, keeping excitation frequency and excitation amplitude constant, it is possible to switch from one state to the other by additional external perturbations. Finally, a conclusion on the numerical and experimental results is given and potential perspectives are outlined.

2. Model

2.1. Equations of motion

We consider a chain of weakly coupled oscillators with a clearance nonlinearity. The clearance nonlinearity offers a simple way to introduce an amplitude dependent stiffening of the individual oscillators, and at the same time actually arises for example in turbomachinery when blade vibrations exceed a certain level. The equation of motion for the nth oscillator may be written down as

$$m\frac{d^2x_n}{dt^2} + c\frac{dx_n}{dt} + F_k(x_n) + k_c(2x_n - x_{n+1} - x_{n-1}) = F_0\cos(\omega t), \tag{1}$$

where x_n is the position of the nth oscillator, m is the mass, c the linear viscous damping coefficient, k_c the coupling stiffness, F_0 the harmonic forcing amplitude with frequency ω and d/dt stands for the derivative with respect to time t. An amplitude dependent restoring force function can be defined as

$$F_k(x_n) = \begin{cases} kx_n; & x_n < g \\ kx_n + k_2(x_n - g); & x_n \geq g \end{cases}, \tag{2}$$

with the clearance or gap g, the linear spring constant k and the additional spring constant k_2, which is activated when the clearance is exceeded, or the gap is closed. To obtain a dimensionless formulation of Eq. (1) we substitute $\tau = \omega_n t$ and $\widetilde{x} = x/x_0$ and introduce the following parameters:

$$\omega_n = \sqrt{\frac{k}{m}}, \quad x_0 = \frac{F_0}{k}, \quad \eta_c = \frac{k_c}{k}, \quad \eta_2 = \frac{k_2}{k}, \quad \xi = \frac{c}{2\sqrt{km}}, \quad \Omega = \frac{\omega}{\omega_n}. \tag{3}$$

The dimensionless equations now read

$$\ddot{\tilde{x}}_n + 2\xi\dot{\tilde{x}}_n + \tilde{F}_k(\tilde{x}_n) + \eta_c(2\tilde{x}_n - \tilde{x}_{n+1} - \tilde{x}_{n-1}) = \cos(\Omega\tau), \tag{4}$$

with

$$\widetilde{F}_k(\widetilde{x}_n) = \begin{cases} \widetilde{x}_n; & \widetilde{x}_n < \widetilde{g} \\ \widetilde{x}_n + \eta_2(\widetilde{x}_n - \widetilde{g}); & \widetilde{x}_n \geq \widetilde{g} \end{cases}, \tag{5}$$

where a superposed dot denotes differentiation with respect to the dimensionless time τ. The mechanical system (Eq. (4)) hence is fully defined by the number of oscillators M, and the dimensionless parameters ξ, η_2,$\widetilde{g}$, η_c and Ω.

2.2. Numerical tools

A widely used method for the computation of periodic solutions is the harmonic balance method, a spectral Galerkin method that employs harmonic base functions as weights [48]. Therefore, the coordinates $\widetilde{x}_i(t)$ are expanded in a truncated Fourier series of order M:

$$\widetilde{x}_n(t) \approx a_{0,n} + \sum_{k=1}^{M} a_{k,n} \cos k\Omega t + b_{k,n} \sin k\Omega t, \tag{6}$$

with the fundamental frequency Ω and the Fourier coefficients a and b. Substituting the expression for $\widetilde{x}_n$, $\dot{\widetilde{x}}_n$ and $\ddot{\widetilde{x}}_n$ into the equations of motion results in a nonlinear algebraic system of equations for the coefficients $(a_{k,n}, b_{k,n})$. The nonlinear vibration analysis tool [49], which comprises numerical continuation and Newton-like solvers was used to solve this system along solution branches via predictor-corrector techniques.

2.3. Single degree of freedom (SDOF)

First we validated the HBM results against time integration for a single degree of freedom (SDOF) oscillator with clearance nonlinearity (i.e. set $\eta_c = 0$ in Eq. (4)). The time integration is performed by using the MATLAB built-in function "ode45" that is based on a Runge-Kutta (4) and (5) formula. The system is defined by the following parameters:

$$\xi = 0.05; \qquad \widetilde{g} = 2; \qquad \eta_2 = 30; \qquad \eta_c = 0. \tag{7}$$

Fig. 1 shows the Frequency Response Function (FRF) in terms of amplitude of the fundamental harmonic $\left|\widetilde{x}^1\right|$ versus the excitation frequency Ω obtained using the HBM with 9 harmonics (black solid line), which proved to be sufficient to provide an accurate solution. Indeed, the restoring force in Eq. (2) is nonlinear and non-smooth hence using a single harmonic to approximate the system dynamics would have led to large errors. Red dots and blue squares were obtained using Time Integration (TI) with sequential continuation, decreasing and increasing the continuation parameter Ω in the range $\Omega = [1, 1.8]$. Fig. 1 shows the accuracy of the HBM implementation. Notice that, due to the clearance nonlinearity, the FRF strongly starts to deviate from the small amplitude linear one at $|\widetilde{x}| \approx |\widetilde{x}^1| = \widetilde{g}$ as the gap closes and the oscillator stiffness increases.

2.4. Weakly coupled chain of oscillators

Now we consider a cyclically symmetric chain of $N = 3$ externally excited oscillators with clearance nonlinearity. Assume that the elements are weakly coupled hence the system parameters in Eq. (4) are

$$\xi = 0.05; \qquad \widetilde{g} = 2; \qquad \eta_2 = 30; \qquad \eta_c = 0.01; \tag{8}$$

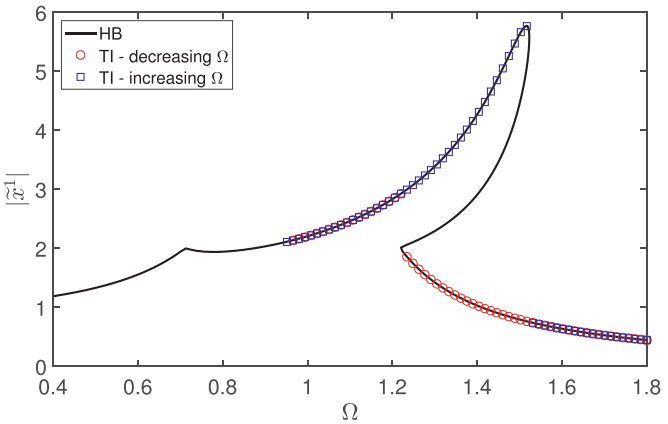

Fig. 1. FRF obtained for a single oscillator using the HB method with 9 harmonics (black line). Red dots and blue squares represent time integration solutions obtained respectively decreasing and increasing Ω. System parameters: $\xi = 0.05, \widetilde{g} = 2, \eta_2 = 30, \eta_c = 0$. (For interpretation of the references to colour in this figure legend, the reader is referred to the web version of this article.)

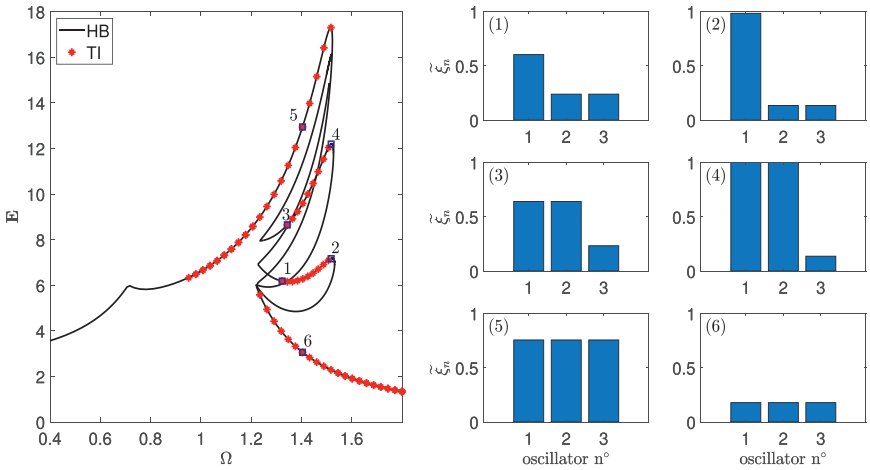

Fig. 2. Left panel: FRF, or bifurcation diagram, of the cyclic symmetric chain of $N = 3$ externally driven weakly coupled oscillators with clearance nonlinearity. Red markers are time integration results, indicating stable states, black solid line HBM results (9 harmonics). System parameters: $\xi = 0.05$, $\eta_2 = 30, \widetilde{g} = 2,\ \eta_c = 0.01$. For the solutions labeled with numbers from (1) to (6) the normalized vibration amplitudes of each oscillator $\widetilde{\xi}_n$ are shown in the plots on the right. (For interpretation of the references to colour in this figure legend, the reader is referred to the web version of this article.)

All the oscillators are excited with an identical external force, equal in magnitude and phase. To visualize the status of the system a scalar parameter $\boldsymbol{E}$ is defined as the sum of the amplitudes of the fundamental harmonics of each oscillator $\left|\widehat{x}_i^1\right|$

$$\boldsymbol{E} = \sum_{i=1}^{N} \left|\widehat{x}_i^1\right|. \tag{9}$$

Fig. 2 shows the system response computed through HBM (9 harmonics, black solid lines) as a function of the excitation frequency Ω, while the red dots have been obtained through time marching simulations (taking the amplitude of the fundamental harmonic via FFT) and help in individuating the stable branches. For $1.2 \lesssim \Omega \lesssim 1.5$ a bifurcation diagram in the form of a typical snaking bifurcation pattern results. From the large and small amplitude homogeneous states, where all oscillators have the same amplitude, a number of additional solution branches arise, comprising both stable and unstable states.

It is revealing to examine the characteristics of these additional states in terms of normalized vibration amplitude. We select six states, which are labeled with the numbers from 1 to 6 in Fig. 2 (left panel) and plot the dimensionless vibration amplitude of each oscillator defined as

$$\widetilde{\xi}_n = \frac{\left|\widetilde{x}_n^1\right|}{X_{\max}}, \tag{10}$$

where $X_{\max}$ is the maximum vibration amplitude across all the six states selected, so that the difference in amplitude between the different solutions can be appreciated (Fig. 2, barplots on the right). Solutions (5) and (6) correspond to homogeneous solutions where the vibration energy is evenly distributed in space, while solutions from (1) to (4) show varying degrees of localization. On the lower branch, solutions (1) to (2), the vibration is mainly localized on a single oscillator, while on the upper branch, solutions (3) to (4), the vibration is mainly localized on two of the three oscillators.

3. Experimental investigation

3.1. System

The cyclic structure under consideration consists of three beams with a common center region, as depicted in Panel (a) of Fig. 3. The structure is made from a 1.5 mm thick aluminium sheet by means of water jet cutting. The beams have width $l_1 = 22$ mm and additional masses are attached to the tips of the beams in a distance $l_2 = 172$ mm from the assembly's center to the centers of the masses. The tip masses measure 25 mm in diameter and 9 mm in height, are glued on both sides of each beam and weigh 35 g each. Two shafts are jointed across the center hole of diameter $d_1 = 13$ mm, as depicted in Panel (a) and (b) of Fig. 3 and thus clamping the center region of the structure while leaving an overhang from $d_2 = 40$ mm to $d_3 = 72$ mm. Note that Panel (b) of Fig. 3 is a schematic drawing of the assembly, and it e.g. leaves out any recesses on the shafts as well as the threaded nuts. The beams are coupled through a slender connection ring, defined by the inner and outer diameters $d_5 = 124$ mm and $d_6 = 134$ mm, respectively, as well as the overhang at the clamping. Increasing the width of these coupling elements leads to an amplified coupling of the beams. A thick disk with a diameter $d_7 = 190$ mm is positioned on one of the shafts in a distance $g \approx 1.5$ mm to the structure. The disk can be positioned on

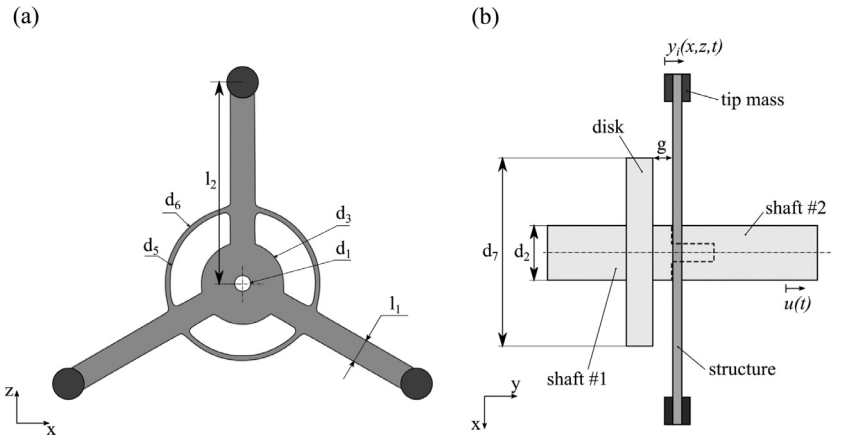

Fig. 3. System with clearance nonlinearity. Panel (a) depicts a drawing of the mounted structure with attached tip masses on each beam. Panel (b) depicts a schematic drawing of the assembly consisting of the structure clamped by the shafts and the mounted disk.

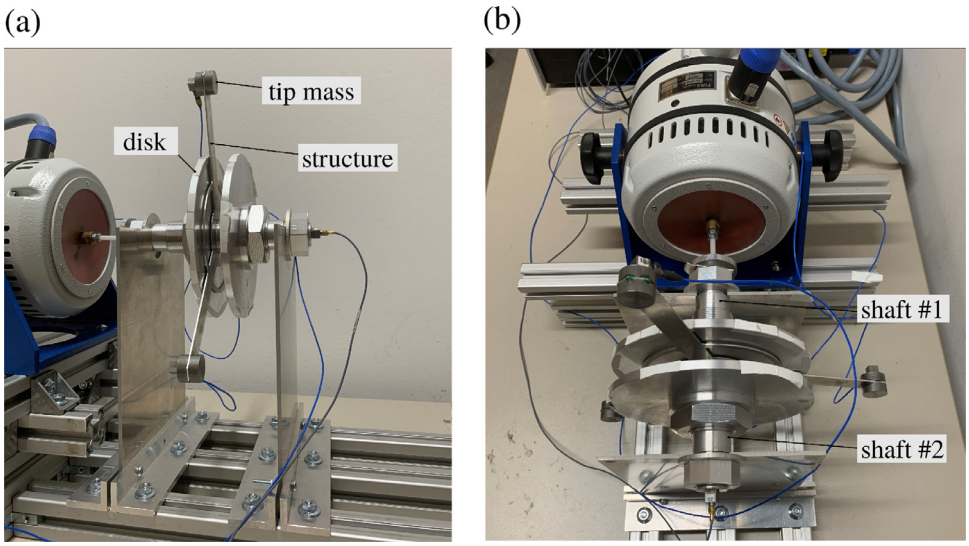

Fig. 4. Test rig with vibration exciter (shaker) attached. Panel (a) side view. Panel (b) top view.

the shafts through a threaded joint and is fixed by a threaded nut. The diameter of the disk and the clearance or gap value control the level of nonlinearity applied to the system. The nonlinearity increases if the clearance is imposed closer to the free end of the beam, since this results in an effectively higher bending stiffness.

The rigid part of the system is built to be moved with a shaker, described in more detail below, to apply an out-of-plane excitation to the structure. Due to the attached tip masses, the beams respond - in the frequency range under consideration - predominantly in their first bending mode $\phi_i(x,z)$ so that from Euler-Bernoulli beam theory their motion can be collected in $y_i(x,z,t)$, where i is the beam number. When the response amplitude surpasses a certain threshold the beams start touching the rigid disks, which effectively increases the restoring force. Hence, as in the model presented in Section 2, the system comprises an amplitude dependent stiffening nonlinearity. Since the beams respond predominantly in their first bending mode the cyclic chain of oscillators in Eq. (1) is a reduced-order model of the system. It is derived by defining $y_i(x,z,t) = \phi_i(x,z)q_i(t)$ with the modal coordinate $q_i(t)$ and applying the Galerkin approximation to the beam equations as in Grolet and Thouverez [37].

The assembly is mounted on two plates by threaded nuts, as depicted in Panel (a) and (b) of Fig. 4. The mounted system is excited by an electrodynamic shaker (TIRA TV 51140-M) and vibrates harmonically due to the first bending mode of the supporting plates. A dSpace controller board (DS1104) with a sampling frequency of 10 kHz processes the excitation signal which is then amplified and fed into the shaker. To measure the response of the system, accelerometers are glued to the three tip masses. Because of memory limitations, appropriate downsampling is applied to the recorded signal. When the system is excited close to the first eigenfrequency the structure starts touching the disk.

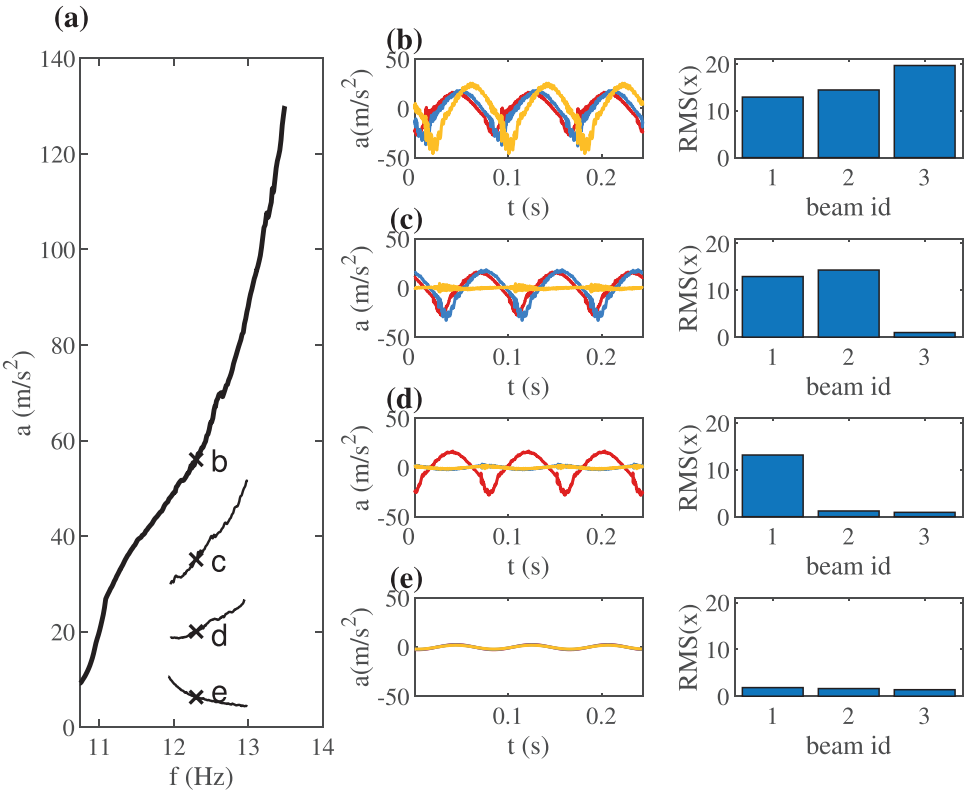

Fig. 5. Frequency response in the nonlinear regime. Panel (a) depicts the different solution branches. Shown is the sum of acceleration amplitudes over the three oscillators. Panel (b)–(e) give the steady state response of the four branches in time domain and the RMS of each signal.

To obtain the modal parameters of a single arm of the structure, a modal hammer test is conducted. First, the disk was positioned far away from the beam and the first eigenfrequency was found at 11.13 Hz with a damping ratio of 5.8%. Next, the disk is positioned in distance g which leads to an eigenfrequency of 13.00 Hz and a damping ratio of 6.0%. Due to manufacturing and assembling a split in frequency was observed for the double mode of the coupled system at 11.04 Hz and 11.11 Hz, while the in-phase mode was identified at 11.24 Hz.

3.2. Results

Panel (a) of Fig. 5 displays the frequency response of the system by plotting the sum of the acceleration amplitudes of the three beams. Sine sweeps were carried out with a sweep rate of ~ 0.0133 Hz/min. The thick line shows the up-sweep starting at 10.90 Hz. At a frequency of ~ 11.08 Hz the structure starts touching the disk and due to the increasing stiffness, a wide resonances shift up to ~ 13.49 Hz is observed. By slight external pertubations of the system at or near about 13 Hz, different stable solutions on different solution branches were triggered. By frequency sweeps these new solutions were followed, and new response branches, represented by the thin lines, were mapped out until they lost stability around ~ 12 Hz.

Panels (b)–(e) show the steady state response of the four solutions marked with crosses in Panel (a). For all states the shaker was driven at constant frequency of 12.30 Hz and identical excitation magnitude. Both the temporal evolution of the signals at the oscillators, as well as the time-averaged (root mean square average) amplitude of the response is depicted. Panels (b) and (e) correspond to the homogenous states, where all beams are in high or low amplitude, respectively. Panel (c) shows a vibration state where two of the oscillators are in large amplitude response, while one is in small amplitude response. Panel (d) shows a vibration state where only one oscillator is in large amplitude response, while the other two are in small amplitude response. The spatial vibration localization caused by the nonlinear characteristics of the system is clearly apparent.

While sweeping through the frequency, the homogeneous state can loose stability and the system configuration becomes localized. Panels (a)–(c) of Fig. 6 plot the acceleration of the three beams in time domain for a linear bidirectional sweep from ~ 12.55 Hz up to 12.9 Hz and back to 12.5 Hz. Panel (d) plots the corresponding RMS in frequency domain, where the squares and triangles mark the forward and backward sweep, respectively. Here, the RMS is computed from the sum of the three acceleration signals and a window of 3937 samples, which corresponds to fifty periods at 12.7 Hz approximately, as the

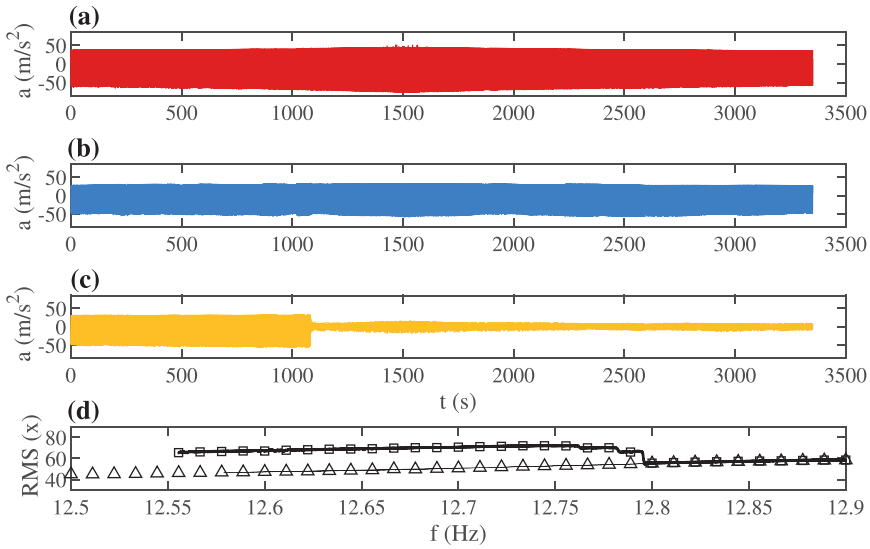

Fig. 6. Linear bidirectional sine sweep starting from homogeneous configuration "111": Panel (a)–(c) depict the acceleration of the three beams. Panel (d) depicts the RMS of the sum of the acceleration signals in frequency domain, where the squares and triangles mark the forward and backward sweep, respectively.

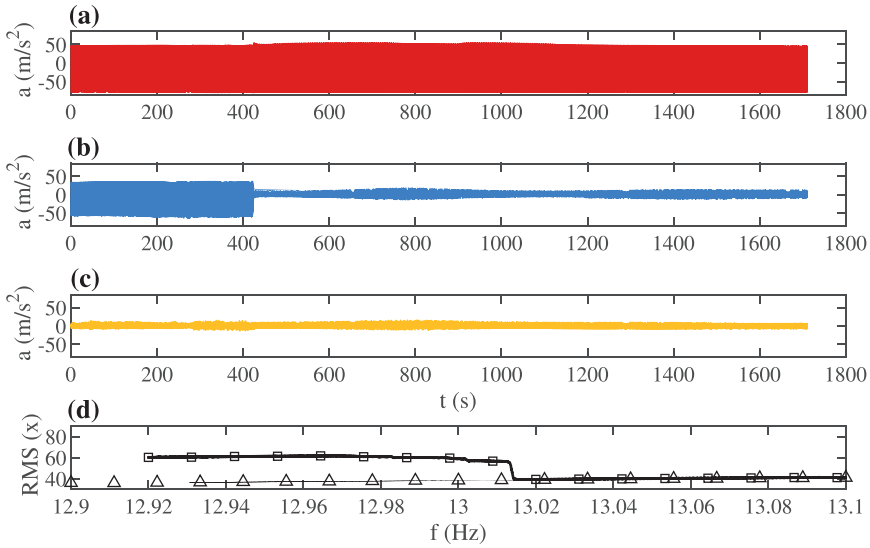

Fig. 7. Linear bidirectional sine sweep starting from localized configuration "110": Panel (a)–(c) depict the acceleration of the three beams. Panel (d) depicts the RMS of the sum of the acceleration signals in frequency domain, where the squares and triangles mark the forward and backward sweep, respectively.

downsampled sampling frequency is 1 kHz. The figure reveals a hysteresis behaviour of the system. At 12.55 Hz the blades are vibrating in high amplitude ("111") up to about $t \simeq 1100$ s, when the third blade vibration amplitude decreases suddenly to a low value. The system remains in the "110" configuration up to the end of the measurement while the excitation frequency sweeps up to 12.9 Hz and goes back to 12.5 Hz.

Next, another linear bidirectional sweep was conducted starting with a configuration of only two beams in high amplitude ("110") from ~ 12.92 Hz up to 13.1 Hz and back to 12.9 Hz, as depicted in Fig. 7. Around $t \simeq 420$ s the second beam suddenly decreases to a low value and the system remains in the "100" configuration up to the end. In here, the RMS was computed by 3846 samples, which corresponds to fifty periods at 13 Hz approximately.

One should note that the revealed types of localization can experimentally be observed on any of the beams, leading to in total six different localized configurations between the two homogenous states. Panels (a) to (c) in Fig. 8 depict the first, second and third beam in large amplitude, while the other beams are in small amplitude. Panels (d)–(f) depict the first, second and third beam in small amplitude, while the other beams are in large amplitude.

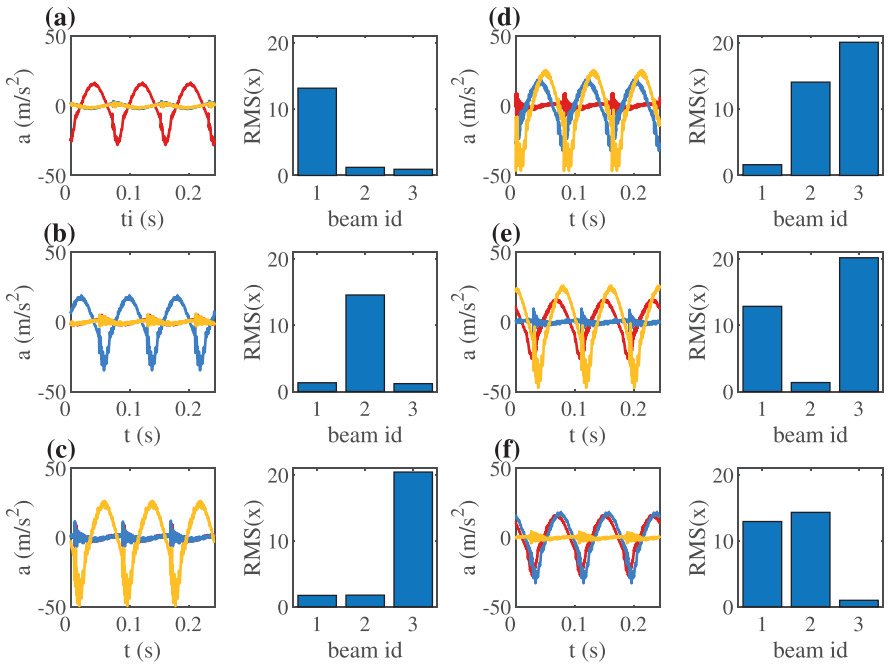

Fig. 8. Different localized configurations in time domain and the corresponding RMS of each signal: Panel (a) to (c) depict the first, second and third beam in large amplitude, while the other beams are in small amplitude. Panel (d)–(f) depict the first, second and third beam in small amplitude, while the other beams are in high amplitude.

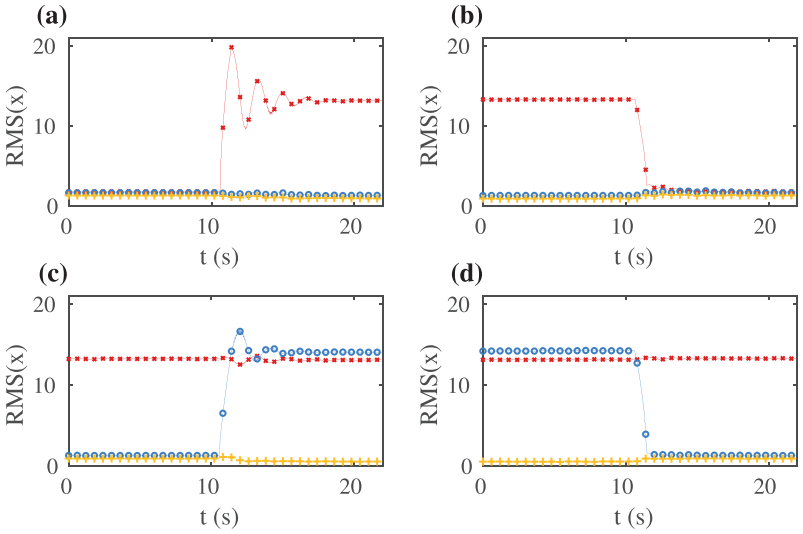

Fig. 9. Transition of localized states in time domain: Panel (a) and (b) depict the transition from the state "000" to "100" and back. Panel (c) and (d) depict the transition from the state "100" to "110" and back.

To experimentally show that the localized states found are stable and somewhat robust, the system was excited at a constant frequency 12.30 Hz and brought in a localized solution. Then it was perturbed so that a different localized solution was reached. Fig. 9 shows the transition in time domain by plotting the upper envelope of the beam acceleration. The envelope is computed as the RMS of the signal with a window of 831 samples, which corresponds to ten periods approximately, as the signal in this experiment was downsampled to a frequency of 1 kHz. Panel(a) and (b) depicts the transition from the homogeneous state with all beams in low amplitude ("000") to the localized state with beam 1 in high amplitude ("100") and back, respectively. The transition from the state "100" to "110" and back is depicted in Panel(c) and (d).

4. Conclusion

In this work, a cyclic chain of weakly coupled oscillators, exposed to a clearance nonlinearity was investigated. A reduced-order model was derived from a structure of three coupled beams through standard Galerkin approximation. Numerical simulation indicated the existence of stable spatially localized vibration states in the nonlinear regime. Motivated from the numerical findings, a test-rig was designed, consisting of three weakly coupled slender beams, each subjected to a clearance nonlinearity. Experimental measurements from the test rig confirm the numerical findings. A frequency sweep displayed the homogenous states with all beams in large or small amplitude, respectively. By deliberate perturbation of the system in the nonlinear regime, all possible configurations of localization could have been obtained. These comprise states with one or two beams in large amplitude and the other beams in small amplitude, accordingly.

The present work has attempted to contribute to the ongoing research on nonlinear vibration localization in cyclic systems. The work provides evidence that the phenomenon of nonlinear vibration localization might actually arise in structures of engineering interest, e.g. turbo-machinery, aero-engines, or wind turbines. Still, more work is needed to better understand the specific conditions of its potential emergence.

As for future work, there are many directions. The present test rig was developed so that it can be adapted to accommodate a larger number of oscillators, which would mean to improve the approximation to realistic system geometries. But also other sorts of nonlinearity will need to be studied, like geometric nonlinearity for large displacements, nonlinear coupling of neighbouring oscillators, or nonlinear aeroelastic coupling by fluid forces.

Declaration of Competing Interest

The authors declare that they have no known competing financial interests or personal relationships that could have appeared to influence the work reported in this paper.

CRediT authorship contribution statement

B. Niedergesäß: Investigation, Writing - original draft, Writing - review & editing. **A. Papangelo:** Investigation, Writing - original draft, Writing - review & editing. **A. Grolet:** Formal analysis, Writing - review & editing. **A. Vizzaccaro:** Methodology, Writing - review & editing. **F. Fontanela:** Methodology, Writing - review & editing. **L. Salles:** Conceptualization, Writing - review & editing. **A.J. Sievers:** Conceptualization, Writing - review & editing. **N. Hoffmann:** Conceptualization, Writing - review & editing.

Acknowledgements

BN thanks E. Groß for guidance and technical support during modal testing. BN and NH thank the DFG (German Research Foundation) under the grant HO 3852 19-1. AP acknowledges the support by the Italian Ministry of Education, University and Research under the Programme Department of Excellence Legge 232/2016 (Grant no. CUP-D94I18000260001). AP is thankful to the DFG (German Research Foundation) for funding the project PA 3303/1-1. AP acknowledges support from "PON Ricerca e Innovazione 2014-2020-Azione I.2" - D.D. n. 407, 27/02/2018, bando AIM (Grant no. AIM1895471). AP acknowledges support from TuTech Innovation GmbH. AJS is supported by a Podell Endowment Award for Research and Scholarship.

References

[1] K.Y. Sanliturk, D.J. Ewins, A.B. Stanbridge, Underplatform dampers for turbine blades: theoretical modelling, analysis and comparison with experimental data, ASME 1999 International gas Turbine and Aeroengine Congress and Exhibition, American Society of Mechanical Engineers, 1999.
[2] C.M. Firrone, S. Zucca, Underplatform dampers for turbine blades: the effect of damper static balance on the blade dynamics, Mech. Res. Commun. 36 (4) (2009) 515–522.
[3] A. Papangelo, M. Ciavarella, On the limits of quasi-static analysis for a simple coulomb frictional oscillator in response to harmonic loads, J. Sound Vib. 339 (2015) 280–289.
[4] A. Papangelo, M. Ciavarella, Optimal normal load variation in wedge-shaped coulomb dampers, J. Strain Anal. Eng. Des. 51 (4) (2016) 279–285.
[5] L. Pesaresi, L. Salles, A. Jones, J.S. Green, C.W. Schwingshackl, Modelling the nonlinear behaviour of an underplatform damper test rig for turbine applications, Mech. Syst. Signal Process. 85 (2017) 662–679.
[6] L. Pesaresi, L. Salles, R. Elliott, A. Jones, J.S. Green, C.W. Schwingshackl, Numerical and experimental investigation of an underplatform damper test rig, Appl. Mech. Mater. 849 (2016) 1–12.
[7] O.O. Bendiksen, Mode localization phenomena in large space structures, AIAA J. 25 (9) (1987) 1241–1248, doi:10.2514/3.9773.
[8] O.O. Bendiksen, P.J. Cornwell, Localization of vibrations in large space reflectors, AIAA J. 27 (2) (1989) 219–226, doi:10.2514/3.10084.
[9] R. Bartels, A. Sayma, Computational aeroelastic modelling of airframes and turbomachinery: progress and challenges, philos, Trans. R. Soc. A 365 (1859) (2007) 2469–2499, doi:10.1098/rsta.2007.2018.
[10] D.J. Ewins, The effects of detuning upon the forced vibrations of bladed disks, J. Sound Vib. 9 (1) (1969) 65–79.
[11] C.H. Hodges, Confinement of vibration by structural irregularity, J. sound Vib. 82 (3) (1982) 411–424.
[12] D.S. Whitehead, Effect of mistuning on the vibration of turbo-machine blades induced by wakes, J. Mech. Eng. Sci. 8 (1) (1966) 15–21.
[13] M.P. Castanier, P. Christophe, Modeling and analysis of mistuned bladed disk vibration: current status and emerging directions, J. Propuls. Power 2 (2006) 384–396.
[14] F. Mashayekhi, A.S. Nobari, S. Zucca, Hybrid reduction of mistuned bladed disks for nonlinear forced response analysis with dry friction, Int. J. Non–Linear Mech. 116 (2019) 73–84.
[15] S.M. Pourkiaee, S. Zucca, A reduced order model for nonlinear dynamics of mistuned bladed disks with shroud friction contacts, J. Eng. Gas Turbines Power 141 (1) (2019) 011031, doi:10.1115/1.4041653.

[16] C. Peng, et al., Non-linear vibration behaviour of an axial compressor rotor blade, in: Proceedings of ASME Turbo Expo 2015, Turbine Technical Conference and Exposition GT2015 June 15, Montreal, Canada, 19, 2015.
[17] I.A. Sever, Nonlinear vibration phenomena in aero-engine measurements, in: Dynamics of Coupled Structures, 4, Springer, Cham, 2016, pp. 241–252.
[18] I.M. Lifshitz, G.I. Stepanova, Vibration spectrum of disordered crystal lattices, Sov. Phys. JETP 3 (5) (1956) 656–662.
[19] P.W. Anderson, Absence of diffusion in certain random lattices, Phys. Rev. 109 (5) (1958) 1492–1505.
[20] A.F. Vakakis, L.I. Manevitch, Y.V. Mikhlin, V.N. Pilipchuk, A.A. Zevin, Normal Modes and Localization in Nonlinear Systems, John Wiley & Sons Inc, New York, 1996.
[21] M. Sato, B.E. Hubbard, A.J. Sievers, B. Ilic, D.A. Czaplewski, H.G. Craighead, Observation of locked intrinsic localized vibrational modes in a micromechanical oscillator array, Phys. Rev. Lett. 90 (4) (2003) 044102.
[22] M. Sato, B.E. Hubbard, A.J. Sievers, Colloquium: nonlinear energy localization and its manipulation in micromechanical oscillator arrays, Rev. Mod. Phys. 78 (1) (2006) 137.
[23] A.J. Dick, B. Balachandran, C.D. Mote, Intrinsic localized modes in microresonator arrays and their relationship to nonlinear vibration modes, Nonlinear Dyn. 54 (1-2) (2008) 13–29.
[24] G. Kerschen, M. Peeters, J.C. Golinval, A.F. Vakakis, Nonlinear normal modes, part I: a useful framework for the structural dynamicist, Mech. Syst. Signal Process. 23 (1) (2009) 170–194, doi:10.1016/j.ymssp.2008.04.002.
[25] A. Papangelo, A. Grolet, L. Salles, N. Hoffmann, M. Ciavarella, Snaking bifurcations in a self-excited oscillator chain with cyclic symmetry, Commun. Nonlinear Sci. Numer. Simul. 44 (2017) 108–119.
[26] A. Papangelo, N. Hoffmann, A. Grolet, M. Stender, M. Ciavarella, M., Multiple spatially localized dynamical states in friction-excited oscillator chains, J. Sound Vib. 417 (2018) 56–64.
[27] M. Didonna, M. Stender, A. Papangelo, F. Fontanela, M. Ciavarella, N. Hoffmann, Reconstruction of governing equations from vibration measurements for geometrically nonlinear systems, Lubricants 7 (8) (2019) 64.
[28] A. Papangelo, F. Fontanela, A. Grolet, M. Ciavarella, N. Hoffmann, Multistability and localization in forced cyclic symmetric structures modelled by weakly-coupled duffing oscillators, J. Sound Vib. 440 (2019) 202–211.
[29] A. Vizzaccaro, L. Salles, C. Peng, Time finite element methods for the periodic solution of blade-tip casing interaction, in: European Conference on Computational Mechanics (ECCM 6), 2018.
[30] A.J. Dick, B. Balachandran, C.D. Mote, Localization in microresonator arrays: influence of natural frequency tuning, J. Comput. Nonlinear Dyn. 5 (1) (2010) 011002.
[31] A.J. Sievers, S. Takeno, Intrinsic localized modes in anharmonic crystals, Phys. Rev. Lett. 61 (8) (1988) 970.
[32] S. Flach, C.R. Willis, Discrete breathers, Phys. Rep. 295 (5) (1998) 181–264.
[33] D.K. Campbell, S. Flach, Y.S. Kivshar, Localizing energy through nonlinearity and discreteness, Phys. Today 57 (2004) 43.
[34] S. Flach, A. Gorbach, Discrete breathers-advances in theory and applications, Phys. Rep. 467 (1) (2008).
[35] A. Papangelo, M. Ciavarella, N. Hoffmann, Subcritical bifurcation in a self-excited single-degree-of-freedom system with velocity weakening-strengthening friction law: analytical results and comparison with experiments, Nonlinear Dyn. 90 (3) (2017) 2037–2046.
[36] A. Papangelo, C. Putignano, N. Hoffmann, Self-excited vibrations due to viscoelastic interactions, Mech. Syst. Signal Process. 144 (2020) 106894.
[37] A. Grolet, F. Thouverez, Free and forced vibration analysis of a nonlinear system with cyclic symmetry: application to a simplified model, J. Sound Vib. 331 (12) (2012) 2911–2928.
[38] F. Fontanela, A. Grolet, L. Salles, A. Chabchoub, N. Hoffmann, Dark solitons, modulation instability and breathers in a chain of weakly non-linear oscillators with cyclic symmetry, J. Sound Vib. 413 (2018) 467–481.
[39] Y. Starosvetsky, L.I. Manevitch, On intense energy exchange and localization in periodic FPU dimer chains, Phys. D 264 (2013) 66–79, doi:10.1016/j.physd.2013.06.012.
[40] M.P. Castanier, C. Pierre, Using intentional mistuning in the design of turbomachinery rotors, AIAA J. 40 (10) (2002) 2077–2086, doi:10.2514/3.15298.
[41] F. Georgiades, M. Peeters, G. Kerschen, J.C. Golinval, M. Ruzzene, Modal analysis of a nonlinear periodic structure with cyclic symmetry, AIAA J. 47 (4) (2009) 1014–1025, doi:10.2514/1.40461.
[42] M.G. Clerc, S. Coulibaly, M.A. Ferré, R.G. Rojas, Chimera states in a duffing oscillators chain coupled to nearest neighbors, Chaos 28 (8) (2018) 083126.
[43] M. Stender, M. Jahn, N. Hoffmann, J. Wallaschek, Hyperchaos co-existing with periodic orbits in a frictional oscillator, J. Sound Vib. 472 (2020) 115203.
[44] A.R. Champneys, Homoclinic orbits in reversible systems and their applications in mechanics, fluids and optics, Phys. D 112 (1) (1998) 158–186.
[45] F. Fontanela, A. Vizzaccaro, J. Auvray, et al., Nonlinear vibration localisation in a symmetric system of two coupled beams, Nonlinear Dyn (2020) https://doi.org/10.1007/s11071-020-05760-x..
[46] O. Thual, S. Fauve, Localized structures generated by subcritical instabilities, J. Phys. 49(11) (1988) 1829–1833.
[47] C. Beaume, A. Bergeon, E. Knobloch, Homoclinic snaking of localized states in doubly diffusive convection, Phys. Fluids 23 (9) (2011) 094102.
[48] J.S. Hesthaven, G. Sigal, G. David, Spectral Methods for Time-Dependent Problems, 21, Cambridge University Press, 2007.
[49] M. Krack, J. Gross, Harmonic Balance for Nonlinear Vibration Problems, Springer, New York, 2019.